Nontrivial Fermi surface topology of the kagome superconductor CsV_3Sb_5 probed by de Haas–van Alphen oscillations

K. Shrestha,[1,*,†] R. Chapai,[2,†] Bal K. Pokharel,[3,4] D. Miertschin,[1] T. Nguyen,[1] X. Zhou,[2] D. Y. Chung,[2] M. G. Kanatzidis,[2,5] J. F. Mitchell,[2] U. Welp,[2] Dragana Popović,[3,4] D. E. Graf,[3,4] B. Lorenz,[6] and W. K. Kwok[2]

[1]*Department of Chemistry and Physics, West Texas A&M University, Canyon, Texas 79016, USA*
[2]*Materials Science Division, Argonne National Laboratory, Lemont, Illinois 60439, USA*
[3]*Department of Physics, Florida State University, Tallahassee, Florida, 32306, USA*
[4]*National High Magnetic Field Laboratory, Tallahassee, Florida 32310, USA*
[5]*Department of Chemistry, Northwestern University, Evanston, Illinois 60201, USA*
[6]*Texas Center for Superconductivity and Department of Physics, University of Houston, 3369 Cullen Boulevard, Houston, Texas 77204, USA*

(Received 12 October 2021; accepted 21 December 2021; published 10 January 2022)

We have investigated the normal state Fermi-surface properties of the kagome superconductor CsV_3Sb_5 using torque magnetometry with applied fields (H) up to 35 T. The torque signal shows clear de Haas–van Alphen (dHvA) oscillations above 15 T. The oscillations are smooth and consist of seven distinct frequencies with values from ∼ 18 T to 2135 T. The presence of higher frequencies in CsV_3Sb_5 is further confirmed by carrying out additional measurements using the tunnel diode oscillator technique. All frequencies measured at different tilt angles (θ) of the field direction with respect to the c axis show a $1/\cos\theta$ dependence, implying that the Fermi surfaces corresponding to these frequencies are two dimensional (2D). The absence of dHvA oscillations at $\theta = 90^o$ further supports the presence of 2D Fermi surfaces. The Berry phase (ϕ) determined from the Landau level fan diagram for all frequencies is ∼ 0.4. This value is close to the theoretical value of $\phi = 0.5$ for a nontrivial system, which strongly supports the nontrivial topology of the Fermi surfaces of these frequencies. Several quantities characterizing the Fermi surface are calculated employing the Lifshitz-Kosevich theory. These findings are crucial for exploring the interplay between nontrivial band topology, charge-density wave, and unconventional superconductivity of CsV_3Sb_5.

DOI: 10.1103/PhysRevB.105.024508

I. INTRODUCTION

The recent discovery of superconductivity (T_c ∼ 0.3–3 K) in a new class of quasi-two-dimensional (2D) kagome metals AV_3Sb_5 (A = K, Rb, and Cs) has attracted enormous attention [1–4]. These materials crystallize in a hexagonal lattice with the $P6/mmm$ space group [1,5]. Transport and magnetization measurements on these materials have shown a clear anomaly at T_{CDW} ∼ 80–110 K arising due to the charge-density wave (CDW) ordering. Theoretical calculations and angle-resolved photoemission spectroscopy (ARPES) have shown that there are several Dirac points near the Fermi level with a nonzero Z_2 topological invariant [1–3]. Therefore, AV_3Sb_5 materials provide unique platforms for exploring the interplay between superconductivity (SC), CDW, and nontrivial band topology [5–8]. Recently, a robust zero-bias conductance peak was observed [9] inside the SC vortex in CsV_3Sb_5 which suggests that this material could be an ideal candidate for topological SC.

Most of the studies in these systems are focused on the SC and its relation with CDW. There exist limited reports [4,10,11] on the Fermi-surface properties, especially via quantum oscillations, although it is one of the crucial methods for investigating the Fermi-surface properties and its topology. The reasons could be the requirements of high-quality single crystals and high magnetic fields (typically above 10 T) to observe Landau level (LL) quantization in AV_3Sb_5. In previous Shubnikov de-Haas (SdH) oscillations studies [10] in CsV_3Sb_5, only low frequencies (below 500 T) were observed. However, recent SdH oscillations studies by Ortiz *et al.* [12] and Fu *et al.* [13] with applied fields up to 14 and 32 T, respectively, showed multiple high frequencies (above 500 T) in addition to the low frequencies reported earlier [10]. Therefore, the exact number of frequencies and hence the Fermi-surface properties of CsV_3Sb_5 are not yet well understood. Moreover, angle dependence, temperature dependence, and Berry phase calculations, which are used to determine the Fermi-surface dimensionality, properties, and topology, have not been performed in previous studies [10,12,13], especially for higher frequencies. Hence, more detailed studies even at higher fields are needed to better understand the Fermi-surface properties and topology of CsV_3Sb_5.

This work focuses on investigating the Fermi surface of CsV_3Sb_5 using torque magnetometry at low temperature down to 0.32 K under applied fields up to 35 T. The torque signal clearly shows the dHvA oscillations with seven distinct frequencies with values ranging from ∼18 to 2135 T, and four of them are above 500 T. The presence of higher frequencies is further confirmed by additional tunnel diode oscillator (TDO) measurements. Our detailed angle dependence of dHvA

*Corresponding author: kshrestha@wtamu.edu
†These authors contributed equally to this work.

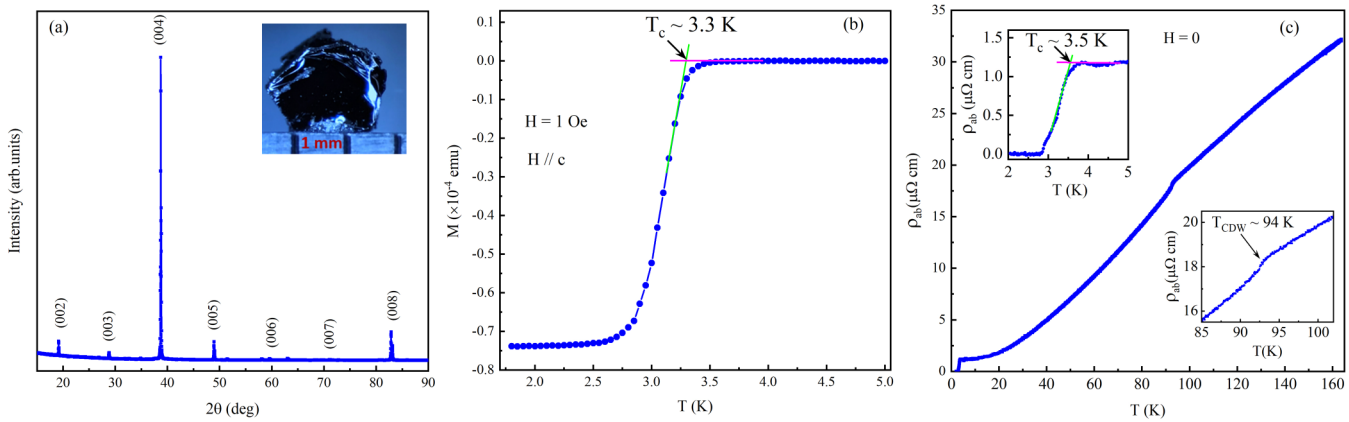

FIG. 1. **XRD, magnetization, and resistivity**. (a) The room-temperature XRD pattern of CsV_3Sb_5 single crystal indexed in the $P6/mmm$ structure. Inset: An optical image of a typical CsV_3Sb_5 single crystal placed beside a millimeter scale. (b) Temperature dependence of magnetization, M(T), measured by applying $H = 1$ Oe along the c axis. (c) Temperature dependence of electrical resistivity ρ_{ab} (T) of CsV_3Sb_5 displaying the CDW transition at 94 K. Upper left inset: ρ_{ab} (T) vs T at low temperature exhibiting the superconducting transition with $T_c \sim 3.5$ K. Lower right inset: ρ_{ab} (T) vs T plot showing the CDW transition, $T_{CDW} \sim 94$ K.

oscillations and Berry phase calculations reveal the presence of 2D Fermi surfaces with nontrivial topology in CsV_3Sb_5.

II. EXPERIMENTAL PROCEDURE

Single crystals of CsV_3Sb_5 were grown via the flux method similar to that described in earlier studies [1,3]. The crystals were then characterized by x-ray diffraction (XRD), magnetization, and resistivity measurements. The XRD measurement was performed in a PANAlytical X'Pert Pro diffractometer. Energy dispersive spectroscopy (EDS) measurements show the near stoichiometry of our single crystals (Fig. S1 in the Supplemental Material [14]). Magnetization measurements were carried out in a magnetic properties measurement system (MPMS-7 T, Quantum Design). Electrical resistivity measurements were performed in a physical properties measurement system (PPMS-9 T, Quantum Design) following a standard four-probe method.

High-field measurements were performed at the National High Magnetic Field Laboratory (NHMFL), Tallahassee, Florida, with applied fields as high as 35 T in a dc resistive water-cooled magnet and top-loaded into a 3-He cryostat allowing for sample temperatures of $\sim$ 0.3 - 60 K. A single crystal of CsV_3Sb_5 was mounted on the rotating platform and slowly cooled down to a base temperature of 0.32 K. The sample was rotated in an applied magnetic field between $H \parallel c$ axis ($\theta = 0^\circ$) and $H \parallel ab$-plane ($\theta = 90^\circ$) in increments of 10°. Magnetic fields were swept at each fixed temperature at a rate of 2.2 T/min. Torque magnetization measurements with a miniature piezoresistive cantilever were used to observe dHvA oscillations where the sample was fixed to the cantilever arm with vacuum grease. Two resistive elements on the cantilever were incorporated with two room-temperature resistors forming a Wheatstone bridge, which was balanced at base temperature before sweeping the magnetic field. A TDO circuit (i.e., self-resonating LC circuit) was used where the sample was placed inside the circuit inductor. The resonant frequency of the circuit is measured, which changes with the magnetic susceptibility of the sample.

III. EXPERIMENTAL RESULTS AND DISCUSSION

Figure 1(a) displays the room-temperature XRD pattern of a CsV_3Sb_5 single crystal indexed in the hexagonal structure with space group $P6/mmm$. An optical image of a typical CsV_3Sb_5 single crystal is presented in the inset of Fig. 1(a). The flat surface corresponds to the ab basal plane, confirmed by XRD which shows (0 0 l) peaks only. Figure 1(b) shows the zero-field cooled temperature dependence of magnetization, M(T) between 1.8 and 5 K measured in an applied magnetic field of 1 Oe along the c axis. A sharp transition in M(T) is observed with an onset of $T_c \sim 3.3$ K. Figure 1(c) shows the temperature dependence of the electrical resistivity, ρ_{ab}(T), measured along the ab plane which exhibits the CDW transition at 94 K (lower right inset) and a SC transition with $T_c \sim 3.5$ K (upper left inset). Both the CDW transition temperature and T_c are consistent with the previously reported values [1,3] for CsV_3Sb_5. Note that $T_c = 3.5$ K we observed here is higher than $T_c = 2.5$ K in the previous reports [1,3].

In order to investigate the Fermi-surface properties of CsV_3Sb_5, we measured the magnetic torque (τ) at very high fields up to 35 T. Figure 2(a) shows the τ vs H plot for two CsV_3Sb_5 single crystals, S1 and S2, at 0.32 K at tilt angle (θ) = 0°. The τ signal increases with H and shows clear dHvA oscillations above 15 T. The quantum oscillations are clearly visible in both S1 and S2, and our calculations showed that both samples have comparable frequencies (Fig. S2 in the Supplemental Material [14]). However, as oscillations are more pronounced in S1 compared with those in S2, we have chosen S1 for further temperature and angle dependence experiments and data analyses. In addition, we rotated the sample in the magnetic field and found that the dHvA oscillations are more pronounced at $\theta = -20^o$. Therefore we have carried out temperature dependence analyses of dHvA oscillations at $\theta = -20^o$. This point is further discussed in the angle dependence data later. Figure 2(b) shows the background subtracted oscillations at $\theta = -20^o$ at different temperatures. The amplitude of oscillations gradually decreases at higher temperatures, and it completely disappears at 60 K. The

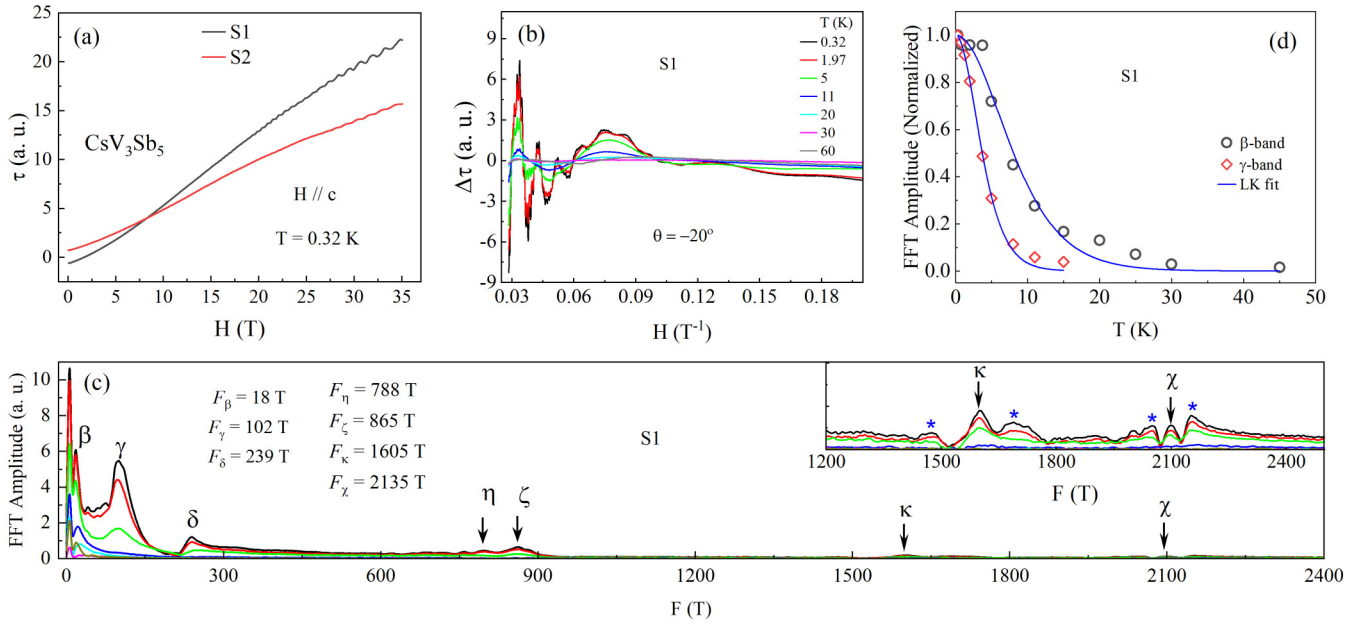

FIG. 2. **dHvA oscillations, Fourier transform, and LK fit**. (a) Magnetic field dependence of magnetic torque (τ) for the two for CsV_3Sb_5 single crystals, S1 and S2, at 0.32 K under applied fields up to 35 T. For both S_1 and S_2, the τ value increases monotonically with the applied field and shows clear dHvA oscillations above 15 T. (b) Background subtracted torque data for S1 at selected temperatures. The amplitude of the oscillations gradually decreases at higher temperatures and completely disappears at 60 K. (c) The frequency spectra of the oscillations data shown in (b). There are seven distinct frequencies ranging from 18 to 2135 T. Inset: The FFT spectra in the range (1200–2500 T) for better visibility of the F_κ and F_χ frequencies. There are a few additional frequencies as denoted by asterisks which disappear quickly at higher temperatures and θ values. (d) Temperature dependence of the FFT amplitudes for the β and γ frequencies. The solid curves represent the best fit to the data using the LK formula [Eq. (1)].

oscillations are smooth, well-defined, and appear to have more than one frequency. The frequency of the dHvA oscillations can be calculated by taking a fast Fourier transform (FFT).

Figure 2(c) shows the Fourier transform of the data shown in Fig. 2(b). There are seven distinct frequencies: Three are low frequencies (F_β = 18 ± 3 T, F_γ = 102 ± 13 T, and F_δ = 239 ± 16 T) and the remaining four (F_η = 788 ± 21 T, F_ζ = 865 ± 23 T, F_κ = 1605 ± 120 T, and F_χ = 2135 ± 90 T) are high frequencies. The low frequencies in CsV_3Sb_5 were already reported by Yu *et al.* [10] using SdH oscillations, and they are in close agreement with our data. There are no published reports of higher frequencies in CsV_3Sb_5 yet. Recently, Fu *et al.* [13] and Ortiz *et al.* [12] claimed the presence of higher frequencies up to 2000 T using SdH oscillations with applied fields up to 32 T. All the frequencies in our dHvA oscillations are in good agreement with those obtained by SdH oscillations [10,12,13]. We noticed that some of the frequencies, especially lower frequencies, in our data were not observed in previous reports [10,12,13] and when observed, the values are slightly different. This small variation could be due to (i) the quality of single crystals, (ii) the different measurement technique we used here (torque magnetometry instead of magnetoresistance) and also could be related to the sensitivity of these measurement techniques, and (iii) these frequencies are at $\theta = -20^o$ not at 0° as in those reports [10,12,13]. The higher frequencies disappear above 8 K, whereas the lower frequencies persist even up to 30 K, which is consistent with recent reports [12,13]. Note that the presence of additional shoulders on either side of the κ and χ frequencies as denoted by the asterisks. These peaks disappear quickly at higher temperatures and θ values. Therefore we could not carry out further analyses to estimate the effective masses and other relevant properties corresponding to them. We noticed that such features were also observed in the FFT spectrum of the previous work [12] and was reported as likely an extrinsic effect. Torque measurements even at higher magnetic fields (above 35 T) might help to resolve the origin of these peaks and understand their Fermi-surface properties.

The frequency (F) of quantum oscillations is directly proportional to the Fermi wave-vector k_F as described assuming circular extremal orbits in Onsager's relation [15,16] $F = \hbar/(2e)k_F^2$, where $\hbar$ is the Planck's constant and k_F is the Fermi wave vector. Therefore, the presence of seven frequencies implies that there are seven Fermi wave vectors corresponding to each frequency and that CsV_3Sb_5 has complex Fermi surfaces with several pockets. In addition, the amplitude of these frequencies decreases at higher temperatures as can be explained by the Lifshitz-Kosevich (LK) formula [15],

$$\Delta\tau(T,H) \propto e^{-\lambda_D}\frac{\lambda(T/H)}{sinh[\lambda(T/H)]}, \qquad (1)$$

with $\lambda_D(H) = \frac{2\pi^2 k_B}{\hbar e} m^* \frac{T_D}{H}$ and $\lambda(T/H) = \frac{2\pi^2 k_B}{\hbar e} m^* \frac{T}{H}$. Here T_D, k_B, and m^* represent the Dingle temperature, Boltzmann's constant, and effective mass of the charge carriers, respectively. The first term is the Dingle factor, which describes attenuation of the oscillations with decreasing field H. The second term explains the weakening of the oscillations at higher temperatures. Due to the presence of multiple frequencies in our data, it is difficult to exactly extract the oscillation

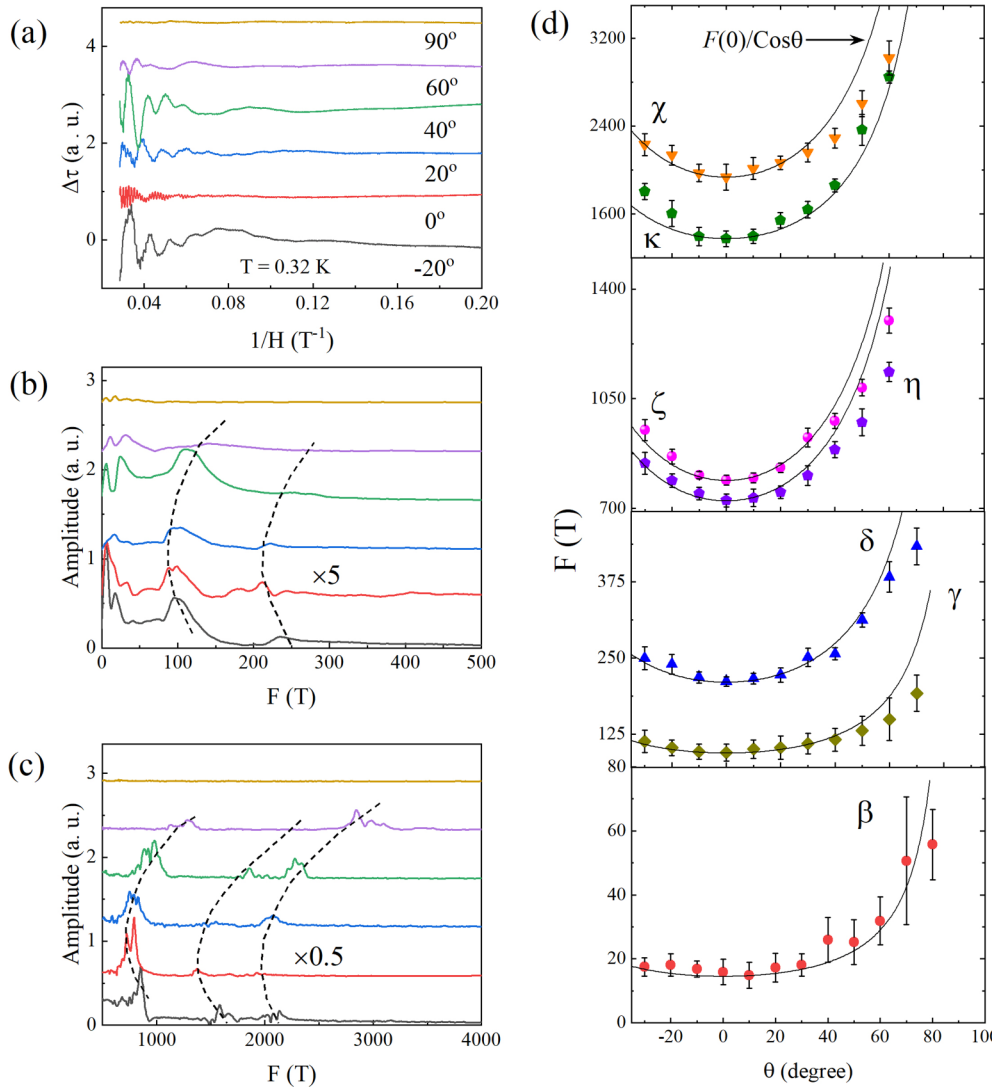

FIG. 3. **Angle-dependent dHvA oscillations**. (a) Background subtracted torque data for CsV_3Sb_5 at selected tilt angles (θ) at 0.32 K. The amplitude of the oscillations decreases at higher θ values and completely disappears at 90°, strongly suggesting the 2D nature of the Fermi surface. The FFT spectrum of the data shown in (a) in the range (b) 0–500 T and (c) 500–4000 T. The FFT data at 0° are multiplied by the factors 5 and 0.5 in (b) and (c), respectively, for better visibility. The curves in (a)–(c) are shifted vertically for clarity. (d) The frequency vs angle plots for all the bands. All frequencies can be clearly resolved up to 70°, and they show $F(0)/\cos\theta$ dependence (solid curves), which strongly suggests that the Fermi surfaces corresponding to these frequencies are 2D. The error bar for each data point in (d) is defined as the half width at half maximum of the respective peak in the frequency plot. The dashed curves are a guide for the eye.

amplitude from raw data [Fig. 2(b)]. Therefore we have taken the temperature dependence of the FFT amplitudes for estimating m^* of the charge carriers. Figure 2(d) shows the normalized FFT amplitudes for the β and γ bands at different temperatures. As seen in the graph, the FFT amplitude decreases with temperature, which can be described by the LK formula [Eq. (1)] as shown by the solid curve. Here the parameter H used in LK fit is taken as 8.75 T, which is the harmonic mean of the inverse fields of the FFT interval [13,17,18]. From the best-fit parameters, we have estimated an effective mass for the β and γ bands to be $m^*_\beta = (0.160 \pm 0.123)m_o$ and $m^*_\gamma = (0.346 \pm 0.065)m_o$, where m_o is the free electron mass. Following the same procedure, we have calculated $m^*_\delta = (0.327 \pm 0.013)m_o$, $m^*_\eta = (0.302 \pm 0.004)m_o$, $m^*_\zeta = (0.312 \pm 0.005)m_o$, $m^*_\kappa = (0.240 \pm 0.009)m_o$, and $m^*_\chi = (0.233 \pm 0.014)m_o$ (Fig. S3 in the Supplemental Material [14]). These mass values are slightly heavier than those reported by Yu *et al.* [10] and Ortiz *et al.* [12] but comparable with those reported by Fu *et al.* [13] for CsV_3Sb_5 (Table S1 in the Supplemental Material [14]). Effective masses reported for other systems (KV_3Sb_5 and RbV_3Sb_5) [4,11] are also comparable with our results.

Angle-dependent dHvA oscillations provide information about the shape, size, and dimensionality of the Fermi surface. Therefore we have rotated the sample *in situ* and measured the torque signal as a function of θ. Figure 3(a) shows the $\Delta\tau$ versus $1/H$ plot for CsV_3Sb_5 at selected θ values. As seen in the graph, the amplitude of the oscillations varies with θ. The oscillations are more pronounced at $\theta = -20^o$ and gradually decrease as we rotate the sample toward $\theta = 0°$. Also the amplitude of these oscillations gradually increases with θ, reaching a maximum near $\theta = 40°$ and then decreases

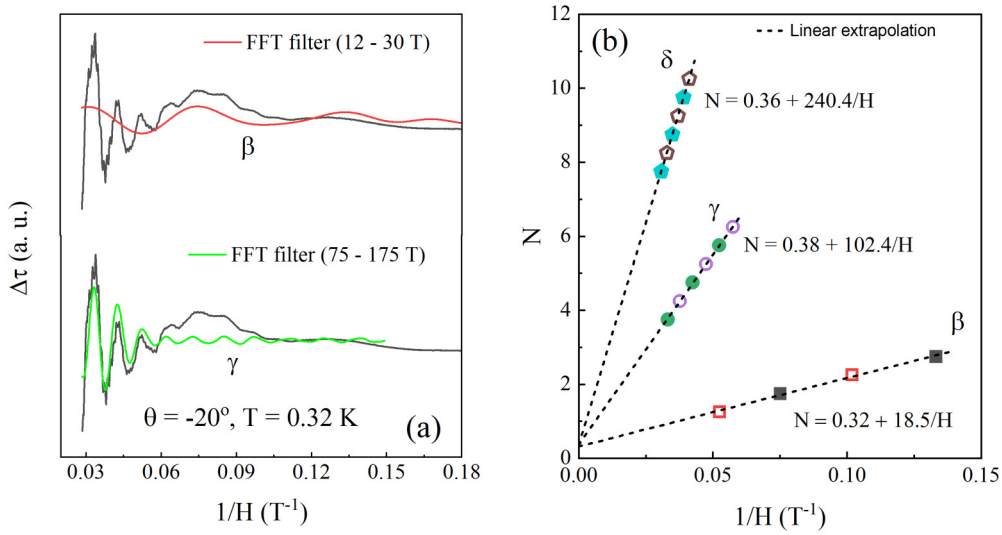

FIG. 4. **The bandpass filter and LL fan diagram.** (a) Separation of the dHvA oscillations corresponding to F_β and F_γ frequencies using the bandpass filters of (12–30 T) and (75–175 T). The black curves are the raw data, and the red and green curves are the filtered data for the β and γ bands, respectively. (b) LL fan diagram for β, γ, and δ frequencies. Minima and maxima of the oscillations are assigned to the $(N + 1/4)$ and $(N - 1/4)$, respectively, for constructing the LL plot. The dashed lines are a linear extrapolation of the data in the limit $1/\mathrm{H} \to 0$.

again at higher θ values. No oscillations are observed at $\theta = 90^\circ$, strongly suggesting the presence of a 2D Fermi surface [16,19,20] in CsV_3Sb_5.

Notice that the period of the dHvA oscillations changes with θ, which means the frequency also varies with θ. Employing a FFT, we have determined the frequencies at different θ values and then presented them in Figs. 3(b) and 3(c). As expected, the frequency changes with θ, as indicated by the dashed lines. No frequencies are observed at $\theta = 90^\circ$ further supporting that the Fermi surfaces are 2D in CsV_3Sb_5.

Angle dependence of the frequencies is plotted in Fig. 3(d). All frequencies (F_β, F_γ, F_δ, F_η, F_ζ, F_κ, and F_χ) vary with θ, as shown in Fig. 3(d). The angle dependence of these frequencies can be described by $F(0)/\cos\theta$, where $F(0)$ is the frequency at $\theta = 0^\circ$, as shown by the solid curves. This provides strong evidence for a 2D Fermi surface [16,19] in CsV_3Sb_5. The cosine dependence of some of the lower frequencies (< 1000 T) in CsV_3Sb_5 has been reported in previous studies [12,13] too. Here we demonstrate that even the higher frequencies (> 1000 T) follow cosine dependence, strongly supporting 2D Fermi surfaces of those frequencies.

Absence of the dHvA oscillations (and frequencies) at $\theta = 90^\circ$ and the cosine dependence of the frequencies already revealed the presence of a 2D Fermi surfaces in CsV_3Sb_5. To solidify this point further, we have estimated the Berry phase (ϕ) which can be calculated by constructing a LL fan diagram [15,16,21]. The ϕ value is π for the topologically nontrivial and 0 for trivial systems [16]. Due to the presence of multiple frequencies, it is not easy to separate the dHvA oscillations for individual frequencies and construct a LL fan diagram. One approach in such a case is to use a bandpass filter and separate the oscillations only corresponding to a specific frequency. This method has been used successfully to determine the ϕ values in many topological systems [22–25]. The solid red and green curves in Fig. 4(a) represent the dHvA oscillations for the β and γ bands separated from raw data (the black curve) using bandpass filters of (12–30 T) and (75–175 T), respectively.

Figure 4(b) shows the LL fan plots for the β, γ, and δ bands. For the dHvA oscillations in magnetization (M), the minima and maxima are assigned $(N - \frac{1}{4})$ and $(N + \frac{1}{4})$, respectively, while constructing the LL fan plot [22,23], where N represents the LL index. Since $\vec{\tau} = \vec{M} \times \vec{H}$, the oscillations in torque signal can be either in or out of phase with the oscillations in magnetization [25]. From the relation [15], $\tau = -\frac{1}{F}\frac{dF}{d\theta}M_\parallel H$, where $M_\parallel$ is the component of M along H, the dHvA oscillations in τ will be in phase with M if the frequency slope is negative ($\frac{dF}{d\theta} < 0$) and out of phase if $\frac{dF}{d\theta} > 0$. In our frequency vs θ plot in Fig. 3(d), all the frequencies show positive slope ($\frac{dF}{d\theta} > 0$). Therefore we have assigned $(N + \frac{1}{4})$ for minima and $(N - \frac{1}{4})$ for maxima in the construction of the LL fan diagram [Fig. 4(b)]. From the linear extrapolation in the limit $1/H \to 0$ in the LL fan diagram, we have obtained $\phi = 0.32 \pm 0.09$, 0.38 ± 0.05, and 0.36 ± 0.01 for the β, γ, and δ bands, respectively. This ϕ value is very close to the theoretical value of 0.5 for a topologically nontrivial system [16,21,26]. In addition, the linear extrapolation gives frequency values of (18.5 ± 0.9) T, (102.4 ± 1.1) T, and (240.4 ± 0.4) T for the β, γ and δ bands, respectively. These frequency values are in close agreement with $F_\beta = 18$ T, $F_\gamma = 102$ T, and $F_\delta = 239$ T obtained from the Fourier transform [Fig. 2(c)]. This implies that the technique of separating the dHvA oscillations using the bandpass filter still preserves the original signal. The ϕ value varies slightly depending on the range of the bandpass filter (Fig. S4 in the Supplemental Material [14]). Therefore we have selected the filter that provides the frequency value that matches the FFT spectrum (Fig. 2). Following the same procedure, we have estimated the ϕ values of ~ 0.4 for the remaining frequencies (Fig. S5 in the Supplemental Material [14]). Recent SdH oscillations studies [13] on CsV_3Sb_5 have also reported nontrivial ϕ values for two of the frequencies (73 and 727 T). The ϕ value close

TABLE I. Physical parameters: The frequency (F), Fermi-surface area (S_F), Fermi wave vector (k_F), effective mass (m^*), Fermi velocity (v_F), Dingle temperature T_D, quantum relaxation time (τ_s), mean-free path (l_{2D}) and quantum mobility (μ), characterizing the dHvA oscillations of CsV_3Sb_5.

Band	F(T)	k_F(Å^{-1})	S_F(Å^{-2})	m^*/m_o	v_F(10^4 ms^{-1})	T_D(K)	τ_s(10^{-13}s)	l_{2D}(nm)	$\mu(m^2V^{-1}s^{-1})$
β	18	0.023	0.172	0.160	16.858	3.2	3.781	63.746	0.414
γ	102	0.056	0.973	0.346	18.558	4.6	2.630	48.815	0.133
δ	239	0.085	2.279	0.327	30.057	4.8	2.521	75.770	0.135
η	788	0.155	7.516	0.302	59.095	0.8	1.512	893.822	0.878
ζ	865	0.162	8.250	0.312	59.931	4.4	2.750	164.811	0.154
κ	1605	0.221	15.308	0.240	106.127	5.9	2.051	217.650	0.150
χ	2135	0.255	20.363	0.233	126.079	1.3	9.308	1173.504	0.701

to 0.5 in our data further confirms nontrivial band topology in CsV_3Sb_5.

From our angle dependence and Berry phase analyses, we have proved the presence of 2D Fermi surfaces in CsV_3Sb_5. To determine various physical parameters characterizing the Fermi surface, we have estimated the Dingle temperature (T_D) for all the bands using the LK formula [Eq. (1)] (Fig. S6 in the Supplemental Material [14]) and listed the values in Table I. Taking the γ band as an example, we have calculated several physical quantities characterizing the Fermi surface. As $F_\gamma = 102$ T using Onsager's relation $F = \hbar/(2e)k_F^2$, the Fermi momentum is $k_F = 0.056$ Å^{-1}. The corresponding Fermi-surface area (S_F) is $\pi k_F^2 = 0.973$ Å^2. Using the linear dispersion relation in 2D, $v_F = \hbar k_F/m^*$, we have estimated the Fermi velocity $v_F = 1.86 \times 10^5$ ms^{-1}. Using the value of $T_D = 4.6$ K, the surface carrier lifetime $\tau = \hbar/2\pi k_B T_D$ is estimated to be $\tau_s = 2.630 \times 10^{-13}$ s. Similarly, other physical parameters like the mean-free path $l_{2D} = v_F\tau_s$ and mobility $\mu = e\tau_s/m^*$ are estimated to be 48.815 nm and 0.133 $m^2V^{-1}s^{-1}$, respectively. There are no reports on AV_3Sb_5 for comparison of these Fermi-surface parameters; however, they are comparable with other topological systems [19,27,28]. Following the same procedure, we have determined those quantities for the remaining bands and tabulated them in Table I. Here we have used the powerful magnetic fields up to 35 T to probe the Fermi-surface properties of CsV_3Sb_5. As described earlier, the minimum fields of 15 T are needed to observe the dHvA oscillations. As the upper critical fields (H_{c2}) [29] for CsV_3Sb_5 are H_{c2} (out of plane) = 0.8 T and H_{c2} (in plane) = 7.2 T, the Fermi-surface properties discussed here represent it at its normal state.

As we mentioned above, we have observed seven distinct frequencies in our dHvA oscillations and four of them are high frequencies (above 500 T) which are not reported in the published data [10] yet. To further confirm the presence of high frequencies in CsV_3Sb_5, we have carried out additional measurements using the TDO technique. This unique technique has been used successfully to investigate the Fermi-surface properties of topological materials in the past [30,31]. Figure 5(a) shows the field dependence of the resonant frequency (δf_{TDO}) with applied fields up to 35 T at 0.32 K and $\theta = 0^\circ$. As seen in the δf_{TDO} vs H plot, there is a clear indication of quantum oscillations above 10 T with several periods. This is further confirmed in the background subtracted data as shown in Fig. 5(b) and inset. To determine the frequencies of the oscillations, we have carried out a Fourier transform of the data which is displayed in (c) and (d). For comparison, we have also included the frequencies obtained from the magnetic torque data at $\theta = 0^\circ$ in (c) and (d). As seen in Figs. 5(c) and 5(d), the frequency spectra obtained from these methods are comparable to one another. Note that there are 10 distinct frequencies in the TDO frequency spectrum: $F_1 = 22$ T, $F_2 = 32$ T, $F_3 = 72$ T, $F_4 = 95$ T, $F_5 = 170$ T, $F_6 = 216$ T, $F_7 = 728$ T, $F_8 = 789$ T, $F_9 = 1400$ T, and $F_{10} = 1751$ T. Some of these frequencies (especially lower frequencies below 500 T) were also observed in previous reports [10,12,13], and their values are comparable to one another. We noticed that there are a few additional frequencies in TDO data which are not clearly defined in our torque measurements. This could be due to different sensitivities of these measurement techniques. Our TDO data further confirm that there exist four higher frequencies with values above 500 T in CsV_3Sb_5. The TDO studies on CsV_3Sb_5 are still in progress, and the detailed results will be reported elsewhere.

IV. SUMMARY

This work presents the normal state Fermi-surface properties of the kagome SC CsV_3Sb_5 using torque magnetometry with applied fields as high as 35 T. The torque signal clearly shows dHvA oscillations with seven distinct frequencies ranging from $\sim$ 18 T to 2135 T. Four frequencies have values above 500 T, which were not observed in the previous publication [10]. The presence of higher frequencies in our data is confirmed by carrying out further high-field measurements using the TDO technique. From the angle dependence of the dHvA oscillations and the Berry phase calculations, we have proved the nontrivial topology of the Fermi surface corresponding to these frequencies in CsV_3Sb_5. Several physical quantities characterizing the Fermi surfaces of CsV_3Sb_5 are calculated using the LK formula and listed in Table I. Although there are some recent Fermi-surface studies in CsV_3Sb_5 using SdH oscillations, this work provides detailed angle dependence, temperature dependence, and Berry phase analyses using dHvA oscillations which helps to better understand the Fermi-surface properties and its topological nature in CsV_3Sb_5.

Note added. During the preparation of this manuscript, we became aware of works by Ortiz *et al.* [12] and Fu *et al.* [13] reporting the observation of high frequencies above 500 T in CsV_3Sb_5 using the SdH oscillations. Fu *et al.* [13] reported four distinct frequencies below 1000 T, whereas Ortiz

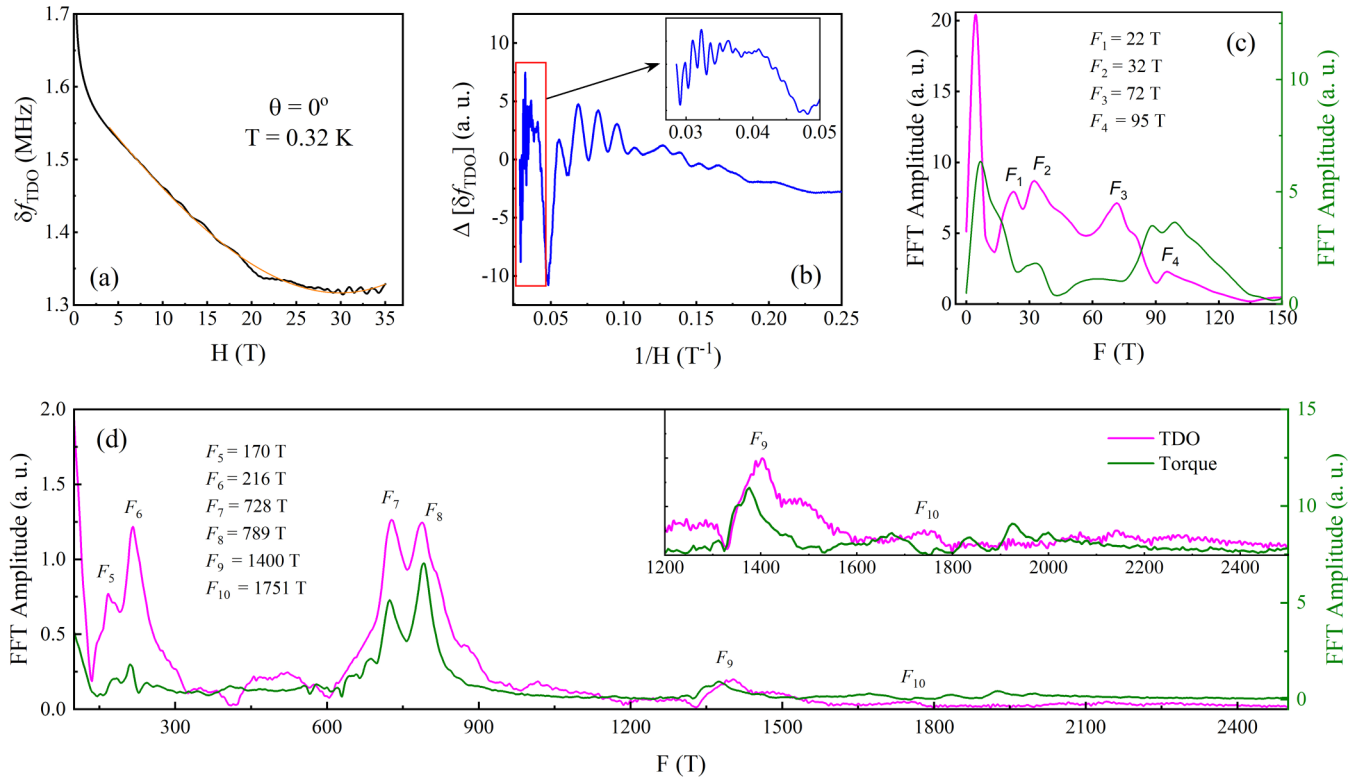

FIG. 5. **TDO.** (a) Resonant frequency, δf_{TDO} vs H data for CsV_3Sb_5 with applied fields up to 35 T at $T = 0.32$ K and $\theta = 0°$. The TDO signal clearly shows oscillations above 10 T. The solid orange curve is the best-fit curve to data using the Chebyshev polynomial for background subtraction. (b) The oscillatory part of the TDO signal after background subtraction. The quantum oscillations are smooth and well defined with different periods. The inset shows zoom-in $1/H$ from 0.027 to 0.05 T^{-1}. The frequency spectra of the oscillations shown in (b) in the range 0 to 150 T (c) and 100 to 2500 T (d). There are ten distinct frequencies ranging from ∼ 4.6 to 1751 T. The frequencies obtained from torque measurements at $\theta = 0°$ are also included for the comparison. The inset in (d) represents the FFT spectra in the range 1200–2500 T for better visibility.

et al. [12] observed nine distinct frequencies up to 2000 T. In their works, the higher frequencies are suppressed quickly at higher angles ($\theta > 20^o$), whereas those frequencies are clearly resolved up to $\theta = 60°$ enabling us to carry out angle dependence measurements to confirm the dimensionality of the Fermi surface.

ACKNOWLEDGMENTS

Sample synthesis, macroscopic characterization, and data analysis (including the dHvA oscillations) performed at Argonne National Laboratory was supported by the U.S. Department of Energy, Office of Science, Basic Energy Sciences, Materials Sciences and Engineering. Quantum oscillations (Torque and TDO) data analyses at West Texas A&M University was supported by the Killgore Faculty Research program and the Welch Foundation (Grant No. AE-0025). A portion of this work was performed at the National High Magnetic Field Laboratory, which is supported by National Science Foundation Cooperative Agreement No. DMR-1644779 and the State of Florida. The work by B.K.P. and D.P. was supported also by NSF Grant No. DMR-1707785.

[1] B. R. Ortiz, L. C. Gomes, J. R. Morey, M. Winiarski, M. Bordelon, J. S. Mangum, I. W. H. Oswald, J. A. Rodriguez-Rivera, J. R. Neilson, S. D. Wilson, E. Ertekin, T. M. McQueen, and E. S. Toberer, New kagome prototype materials: discovery of KV_3Sb_5, RbV_3Sb_5, and $C_SV_3Sb_5$, Phys. Rev. Materials **3**, 094407 (2019).

[2] B. R. Ortiz, P. M. Sarte, E. M. Kenney, M. J. Graf, S. M. L. Teicher, R. Seshadri, and S. D. Wilson, Superconductivity in the $\mathbb{Z}_2$ kagome metal KV_3Sb_5, Phys. Rev. Materials **5**, 034801 (2021).

[3] B. R. Ortiz, S. M. Teicher, Y. Hu, J. L. Zuo, P. M. Sarte, E. C. Schueller, A. M. Abeykoon, M. J. Krogstad, S. Rosenkranz, R. Osborn, R. Seshadri, L. Balents, J. He, and S. D. Wilson, $C_SV_3Sb_5 : A\mathbb{Z}_2$ Topological Kagome Metal with a Superconducting Ground State, Phys. Rev. Lett. **125**, 247002 (2020).

[4] Q. Yin, Z. Tu, C. Gong, Y. Fu, S. Yan, and H. Lei, Superconductivity and normal-state properties of kagome metal RbV_3Sb_5 single crystals, Chin. Phys. Lett. **38**, 037403 (2021).

[5] K. Jiang, T. Wu, J.-X. Yin, Z. Wang, M. Z. Hasan, S. D. Wilson, X. Chen, and J. Hu, Kagome superconductors AV_3Sb_5 (A=K,Rb,Cs), arXiv:2109.10809.

[6] F. H. Yu, D. H. Ma, W. Z. Zhuo, S. Q. Liu, X. K. Wen, B. Lei, J. J. Ying, and X. H. Chen, Unusual competition of

superconductivity and charge-density-wave state in a compressed topological kagome metal, Nat. Commun. **12**, 3645 (2021).

[7] K. Y. Chen, N. N. Wang, Q. W. Yin, Y. H. Gu, K. Jiang, Z. J. Tu, C. S. Gong, Y. Uwatoko, J. P. Sun, H. C. Lei, J. P. Hu, and J. G. Cheng, Double Superconducting Dome and Triple Enhancement of T_c in the Kagome Superconductor CsV_3Sb_5 Under High Pressure, Phys. Rev. Lett. **126**, 247001 (2021).

[8] N. N. Wang, K. Y. Chen, Q. W. Yin, Y. N. N. Ma, B. Y. Pan, X. Yang, X. Y. Ji, S. L. Wu, P. F. Shan, S. X. Xu, Z. J. Tu, C. S. Gong, G. T. Liu, G. Li, Y. Uwatoko, X. L. Dong, H. C. Lei, J. P. Sun, and J.-G. Cheng, Competition between charge-density-wave and superconductivity in the kagome metal RbV_3Sb_5, Phys. Rev. Research **3**, 043018 (2021).

[9] Z. Liang, X. Hou, F. Zhang, W. Ma, P. Wu, Z. Zhang, F. Yu, J.-J. Ying, K. Jiang, L. Shan, Z. Wang, and X.-H. Chen, Three-Dimensional Charge Density Wave and Surface-Dependent Vortex-Core States in a Kagome Superconductor CsV_3Sb_5, Phys. Rev. X **11**, 031026 (2021).

[10] F. H. Yu, T. Wu, Z. Y. Wang, B. Lei, W. Z. Zhuo, J. J. Ying, and X. H. Chen, Concurrence of anomalous hall effect and charge density wave in a superconducting topological kagome metal, Phys. Rev. B **104**, L041103 (2021).

[11] S.-Y. Yang, Y. Wang, B. R. Ortiz, D. Liu, J. Gayles, E. Derunova, R. Gonzalez-Hernandez, L. Šmejkal, Y. Chen, S. S. P. Parkin, S. D. Wilson, E. S. Toberer, T. McQueen, and M. N Ali, Giant, unconventional anomalous hall effect in the metallic frustrated magnet candidate, KV_3Sb_5, Sci. Adv. **6**, eabb6003 (2020).

[12] B. R. Ortiz, S. M. L. Teicher, L. Kautzsch, P. M. Sarte, N. Ratcliff, J. Harter, J. P.C. Ruff, R. Seshadri, and S. D. Wilson, Fermi surface mapping and the nature of charge density wave order in the kagome superconductor CsV_3Sb_5, Phys. Rev. X **11**, 041030 (2021).

[13] Y. Fu, N. Zhao, Z. Chen, Q. Yin, Z. Tu, C. Gong, C. Xi, X. Zhu, Y. Sun, K. Liu, and H. Lei, Quantum transport evidence of topological band structures of kagome superconductor CsV_3Sb_5, Phys. Rev. Lett. **127**, 207002 (2021).

[14] See Supplemental Material at http://link.aps.org/supplemental/10.1103/PhysRevB.105.024508 for the detail information on EDS analyses, Berry phase calculations, Lifshitz-Kosevich fits, Dingle-temperature analyses, etc.

[15] D. Shoenberg, *Magnetic Oscillations in Metals* (Cambridge University Press, 1984).

[16] K. Shrestha, V. Marinova, D. Graf, B. Lorenz, and C. W. Chu, Quantum oscillations in metallic Sb_2Te_2Se topological insulator, Phys. Rev. B **95**, 075102 (2017).

[17] D. Rhodes, S. Das, Q. R. Zhang, B. Zeng, N. R. Pradhan, N. Kikugawa, E. Manousakis, and L. Balicas, Role of spin-orbit coupling and evolution of the electronic structure of WTe_2 under an external magnetic field, Phys. Rev. B **92**, 125152 (2015).

[18] K. Shrestha, V. Marinova, D. Graf, B. Lorenz, and C. W. Chu, Large magnetoresistance and fermi surface study of Sb_2Se_2Te single crystal, J. Appl. Phys. **122**, 125901 (2017).

[19] D.-X. Qu, Y. S. Hor, J. Xiong, R. J. Cava, and N. P. Ong, Quantum oscillations and hall anomaly of surface states in the topological insulator Bi_2Te_3, Science **329**, 821 (2010).

[20] K. Shrestha, V. Marinova, B. Lorenz, and P. C. W. Chu, Shubnikov-de haas oscillations from topological surface states of metallic $Bi_2Se_{2.1}Te_{0.9}$, Phys. Rev. B **90**, 241111(R) (2014).

[21] K. Shrestha, D. E. Graf, V. Marinova, B. Lorenz, and P. C. W. Chu, Simultaneous detection of quantum oscillations from bulk and topological surface states in metallic $Bi_2Se_{2.1}Te_{0.9}$, Phil. Mag. **97**, 1740 (2017).

[22] W. Zheng, R. Schönemann, N. Aryal, Q. Zhou, D. Rhodes, Y.-C. Chiu, K.-W. Chen, E. Kampert, T. Förster, T. J. Martin, G. T. McCandless, J. Y. Chan, E. Manousakis, and L. Balicas, Detailed study of the fermi surfaces of the type-ii dirac semimetallic candidates XTe_2 (X = Pd, Pt), Phys. Rev. B **97**, 235154 (2018).

[23] W. Zheng, R. Schönemann, S. Mozaffari, Y.-C. Chiu, Z. B. Goraum, N. Aryal, E. Manousakis, T. M. Siegrist, K. Wei, and L. Balicas, Bulk fermi surfaces of the dirac type-ii semimetallic candidate $NiTe_2$, Phys. Rev. B **102**, 125103 (2020).

[24] M. A. Khan, D. E. Graf, I. Vekhter, D. A. Browne, J. F. DiTusa, W. A. Phelan, and D. P. Young, Quantum oscillations and a nontrivial berry phase in the noncentrosymmetric topological superconductor candidate BiPd, Phys. Rev. B **99**, 020507(R) (2019).

[25] R. Chapai, D. A. Browne, D. E. Graf, J. F. DiTusa, and R. Jin, Quantum oscillations with angular dependence in $PdTe_2$ single crystals, J. Phys.: Condens. Matter **33**, 035601 (2021).

[26] K. Shrestha, V. Marinova, B. Lorenz, and C. W. Chu, Evidence of a 2D fermi surface due to surface states in a p-type metallic Bi_2Te_3, J. Phys.: Condens. Matter **30**, 185601 (2018).

[27] A. A. Taskin, Z. Ren, S. Sasaki, K. Segawa, and Y. Ando, Observation of Dirac Holes and Electrons in a Topological Insulator, Phys. Rev. Lett. **107**, 016801 (2011).

[28] J. G. Analytis, R. D. McDonald, S. C. Riggs, J.-H. Chu, G. S. Boebinger, and I. R. Fisher, Two-dimensional surface state in the quantum limit of a topological insulator, Nat. Phys. **6**, 960 (2010).

[29] S. Ni, S. Ma, Y. Zhang, J. Yuan, H. Yang, Z. Lu, N. Wang, J. Sun, Z. Zhao, D. Li, S. Liu, H. Zhang, H. Chen, K. Jin, J. Cheng, L. Yu, F. Zhou, X. Dong, J. Hu, H.-J. Gao, and et al., Anisotropic superconducting properties of kagome metal CsV_3Sb_5, Chin. Phys. Lett. **38**, 057403 (2021).

[30] Y. Obata, Y. Kohama, S. Matsuishi, and H. Hosono, Shubnikov-de haas oscillations in the three-dimensional dirac fermion system Ca_3PbO, Phys. Rev. B **99**, 115133 (2019).

[31] J. Song, B. C. Park, K. I. Sim, J. Bang, S. Kim, Z. Yang, Y. Kohama, Y. Kim, and S. W. Kim, Tunable berry curvature and transport crossover in topological dirac semimetal KZnBi, npj Quan. Mater. **6**, 77 (2021).